applied sciences

MDPI

Article

Mitigation of Structural Vibrations of MDOF Oscillators by Modal Coupling Due to Hysteretic Dampers

Paolo Casini * and Fabrizio Vestroni

Department of Structural and Geotechnical Engineering, Sapienza University of Rome, 00184 Rome, Italy
* Correspondence: p.casini@uniroma1.it

Abstract: In civil engineering, structural elements characterized by hysteresis are often encountered, such as materials with limited elastic fields, microsliding friction and elastomeric absorbers. Hysteretic nonlinearities produce a wide variety of dynamical phenomena, such as significant modal coupling, bifurcations and superabundant modes. This paper investigates nonlinear modal interactions in the dynamic response of a two-degree-of-freedom system (2DOF) with hysteretic elements. These phenomena are notably important in internal resonance conditions, where modal interactions produce strong modifications in the response with possible beneficial effects. In specific conditions, the transfer of energy between the two modes leads to a notable reduction in the maximum response amplitude; the exploitation of this feature to achieve vibration mitigation of the forced response is the main goal of the paper. Two configurations are investigated: the hysteretic element at the top (vibration damper) and the hysteretic element at the base (isolator). In both cases, several internal resonance conditions occur since, by increasing the excitation intensity, the frequencies of the hysteretic system change, as well as their ratio. Qualitative similar results are obtained, characterized by a transfer of energy between the two modes. For both configurations, the usefulness of exploiting these nonlinear phenomena in vibration mitigation has been shown.

Keywords: hysteresis; internal resonances; nonlinear modal interaction; vibration mitigation

check for updates

Citation: Casini, P.; Vestroni, F. Mitigation of Structural Vibrations of MDOF Oscillators by Modal Coupling Due to Hysteretic Dampers. *Appl. Sci.* **2022**, *12*, 10079. https://doi.org/10.3390/app121910079

Academic Editor: Felix Weber

Received: 27 July 2022
Accepted: 29 September 2022
Published: 7 October 2022

Publisher's Note: MDPI stays neutral with regard to jurisdictional claims in published maps and institutional affiliations.

Copyright: © 2022 by the authors. Licensee MDPI, Basel, Switzerland. This article is an open access article distributed under the terms and conditions of the Creative Commons Attribution (CC BY) license (https://creativecommons.org/licenses/by/4.0/).

1. Introduction

In the last decades, great interest has been given to the dynamic phenomena typical of nonlinear systems in view of exploiting them to mitigate the effects of dynamic excitations [1–4]. One of the usual techniques used to reduce structural vibration is to introduce elements that guarantee a higher dissipation capacity [5]; here, the choice of introducing hysteretic elements allows the combination of two strategies, which increase the ability of the structure to dissipate energy and, at the same time, exploit the beneficial aspects of the nonlinear dynamic coupling caused by the hysteresis itself [6–9].

The variety of the nonlinear phenomena is very large [10]; in particular, the modification of the modal quantities, with the oscillation amplitude, assumes great importance and entails change in the natural frequencies and in the linear modes. They are no longer orthogonal, and in a periodic cycle, they change their shape, leading to modal trajectories that are no longer straight in the configuration plane [11,12]. The occurrence of internal resonance conditions is easily met, and in these conditions, the modal coupling is exalted [4,7].

Several nonlinear motions can take place, such as multifrequencies or quasiperiodic and chaotic oscillations [10,13,14]; however, the attention here is focused on more robust phenomena related to periodic motion and features related to cases of strong nonlinearities. Under these conditions, an unusual phenomenon occurs when a novel mode arises with respect to the linear ones, as already observed in [7,11,15,16].

Hysteretic behavior is widespread among materials and elements; it is easily encountered in civil, mechanical, aeronautical and electrical engineering, and it is characterized by an intrinsic capacity for energy dissipation [6–9,17,18]. Some examples are materials

with limited elastic fields, elastomeric absorbers, shape-memory alloys, contacts exhibiting microsliding friction and magnetostrictive materials. Compared to geometric nonlinearities, those introduced by hysteresis can produce more marked effects on the dynamic response [14,17–22] and give rise to phenomena typical of nonlinear dynamics, such as modal coupling, bifurcations and the emergence of superabundant modes [12,16,23,24].

A system is said to be endowed with hysteresis if the output depends, in a rate-independent way, on the history of the input [25]; however, this definition does not consider that rate-dependent hysteresis can be encountered in a number of applications involving smart materials, piezoelectric actuators or other specific devices [26]. According to this definition, the main characteristic of hysteresis is thus its dependence on the history of the input; while rate independence relatively eases the treatment of the problem, the dependence on the history makes it very difficult to obtain analytically tractable formulations. Thus, beyond the high number of different restoring forces encountered in the real world, this explains the high number of models proposed in the literature, even when limited to the mechanical field. Among the differential models, the Bouc–Wen model [27,28] was adopted because it is very versatile in describing various hysteretic behaviors and simple due to its ability to give analytical piecewise smooth representations of stress–strain relationships. The versatility of the model in describing restoring forces with different characteristics has been demonstrated in several papers [14,29–31]; however, here, the Bouc–Wen law was adopted in its basic formulation because the interest is mainly devoted to exploiting the use of generic hysteretic behaviors for vibration mitigation.

For this aim, a 2DOF system with one hysteretic element, representative of a multidegree-of-freedom system under harmonic excitation, was investigated. Two configurations were considered: in the first, the hysteretic element was between the two masses, and in the second, it was between the base and the first mass, developing and enlarging the results already obtained separately in [4,7] and updating the cases developed in [32] with specific attention to vibration mitigation. The favorable effects in the mitigation of the system response through the combined use of the nonlinear dynamic phenomena and the high dissipation capacity of hysteretic elements were illustrated, showing a very promising area for structural applications.

2. Response to Harmonic Excitation of a Hysteretic SDOF Oscillator

Several models have been proposed in the literature to represent hysteretic behavior. For its simplicity and versatility, the differential model by Bouc–Wen is used here; by properly tuning the model parameters, it is possible to capture the real mechanical characteristics of many mechanical devices with hysteresis [29–31].

A single-degree-of-freedom (SDOF) oscillator with Bouc–Wen hysteresis and under harmonic excitation was first investigated, Figure 1a. The mass m_1 was connected to the moving support by an element that provides a restoring force f due to an elastic and a hysteretic component:

$$f = k_1 x_1 + z \tag{1}$$

The elastic component was characterized by stiffness k_1, whereas the hysteretic part z was provided by the Bouc–Wen law by solving the following nonlinear differential equation:

$$\frac{dz}{dt} = \left\{ k_d - \left[\gamma + \beta \, sgn\left(z \frac{dx_1}{dt} \right) \right] |z|^n \right\} \frac{dx_1}{dt} \tag{2}$$

where k_d, γ, β, n are the constitutive parameters of the Bouc–Wen law.

The element stiffness depended on the oscillation amplitude, which varied from an initial value $k_A = k_1 + k_d$ to a final value k_B corresponding to the post-elastic stiffness, $k_B = k_1$, Figure 1b. The yield-restoring force f_y and the yield displacement $x_y = f_y / k_A$ are reported in Figure 1b. The ratio between the final and initial stiffness values is defined as the hardening coefficient and denoted by δ: $\delta = k_B / k_A$. The parameter n in Equation (2) defines the degree of smoothness of the transition from the elastic to post-elastic branches

and is assumed here to be unitary, as in most mechanical applications. The parameters β and γ tune the extent of the restoring force loop; more precisely, their sum $(\beta + \gamma)$ affects the maximum value of the hysteretic force, while their ratio γ/β controls the shape of the cycles and, consequently, the dissipative capacity of the element, Figure 1c. In particular, for fixed $(\beta + \gamma)$, the maximum loop area, and therefore, the maximum energy dissipation is obtained when $\gamma = \beta$ [7]; under this condition, the restoring force is defined as fully hysteretic. For $\frac{\gamma}{\beta} > 1$, there is a smaller cycle area and, therefore, decreasing dissipated energy; a reduced hysteresis is said to occur in this case.

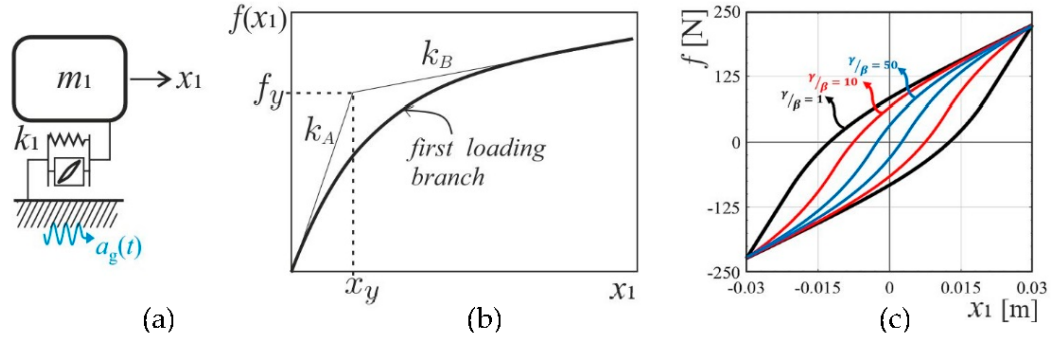

Figure 1. (**a**) SDOF Bouc–Wen oscillator; (**b**) first loading branch; (**c**) restoring force loops for $\gamma/\beta = 1$, 10, 50.

The equation of motion of a SDOF under a harmonic base excitation, which is characterized by amplitude a_g and frequency Ω, is:

$$m_1 \frac{d^2 x_1}{dt^2} + k_1 x_1 + z = -m_1 a_g \sin(\Omega t) \tag{3}$$

where z is provided by Equation (2). It is useful to introduce some quantities related to the parameters of the Bouc–Wen hysteretic element with clear mechanical meanings, such as the hardening coefficient δ, the yield strength f_y and the yield displacement x_y. These can be expressed as:

$$\delta = \frac{k_B}{k_A}, \quad f_y = \frac{k_A}{k_d}\left(\frac{k_d}{\beta + \gamma}\right)^{\frac{1}{n}}, \quad x_y = \frac{f_y}{k_A}, \tag{4}$$

Additionally, the initial and final frequency, ω_A and ω_B, which are associated with small and large oscillation amplitudes, the adimensional force intensity A and the driven frequency η are defined as:

$$\omega_A = \sqrt{\frac{k_A}{m}}, \quad \omega_B = \sqrt{\frac{k_B}{m}}, \quad A = \frac{m a_g}{f_y}, \quad \eta = \frac{\Omega}{\omega_A} \tag{5}$$

As demonstrated in [4], the stiffness and damping characteristics of the hysteretic absorber depend on the vibration amplitude $\bar{x}$. In particular, the equivalent stiffness k_e as a function of $\bar{x}$ can be expressed in the following form:

$$k_e(\bar{x}) = k_1 + \frac{k_d}{\bar{x}(\beta + \gamma)}\left(1 - e^{-\bar{x}(\beta+\gamma)}\right) \tag{6}$$

According to Equation (6), it decreases with the excitation intensity varying from k_A to k_B. To characterize the damping properties, the equivalent damping coefficient ζ_e was introduced and defined as the value of damping of a viscoelastic oscillator that dissipates the same energy E_{BW} of the hysteretic device in an oscillation with the same frequency and amplitude $\bar{x}$:

$$\zeta_e(\bar{x}) = \frac{E_{BW}}{2\pi k_e \bar{x}^2} \tag{7}$$

The frequency response curves (FRCs) of the hysteretic SDOF (Table A1 in the Appendix A) with $\gamma/\beta = 1,\ 10$ are reported in Figure 2a,b for increasing values of the excitation intensity. In Figure 2a the case of full hysteresis (BW1) is illustrated. The nonlinearity of hysteresis is of the softening type, and the frequency–amplitude curve drawn by the resonance peaks is bent on the left. The nonlinear frequency of the oscillator is close to ω_A for low amplitudes and decreases, moving towards the post-elastic frequency ω_B for increasing response amplitudes. The curves are made by stable periodic solutions; the branch nearly vertical which connects the non-resonant and resonant branches is marginally stable [33].

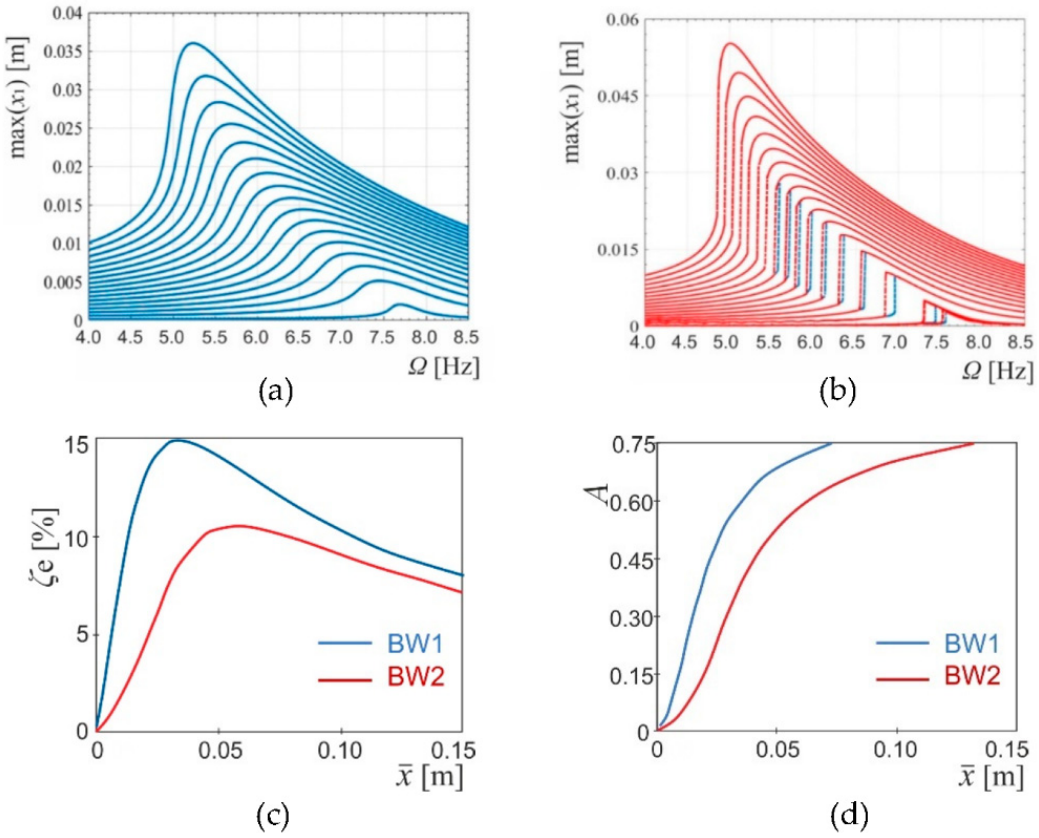

Figure 2. SDOF oscillator: frequency–response curves for varying excitation intensity: (**a**) $\gamma/\beta = 1$, A = 0.01–0.63; (**b**) $\gamma/\beta = 10$, A = 0.01–0.57 (ω_A = 7.83 Hz, ω_B = 4.31 Hz); (**c**) equivalent damping coefficient ζ_e vs. response amplitude; (**d**) excitation intensity vs. response amplitude.

Figure 2b shows a response with reduced hysteresis loops, $\gamma/\beta = 10$ (BW2). For the same excitation intensity, greater response amplitudes are obtained at resonance with respect to the previous case BW1, as evident in Figure 2d. This is expected behavior related to a lower level of equivalent damping, Figure 2c. A more specific difference is the coexistence of the resonant and non-resonant branches in a small range of frequency, leading to multivalued curves with the classical jump phenomenon. This range of coexisting solutions widens with γ/β, while disappearing with increasing force intensity, as evidenced by different constitutive laws [33]; this is because the dissipation capacity between full and reduced hysteresis is not more appreciable at high amplitudes.

The trend of the equivalent damping coefficient ζ_e versus the response amplitude (Equation (7)) is reported in Figure 2c for fully and reduced hysteretic systems; ζ_e increases with amplitude, reaches a maximum, and then decreases, which means that in the intermediate range of amplitudes, the dissipation capacity is greater. This is the reason why, although the equivalent stiffness decreases with amplitude, the relation between force and resonance response amplitude is steeper with respect to the ranges of small and large values, Figure 2d.

3. 2DOF Systems with Hysteretic Dampers

The phenomena of nonlinear modal interactions in a multidegree-of-freedom system can be suitably investigated by means of a 2DOF oscillator [7,24]. The analysis was developed for two different realizations: (a) top configuration (Figure 3a), where the second element was hysteretic, and the goal was to reduce the response of the main mass m_1 and (b) base configuration (Figure 3b), where the first element was hysteretic, and the goal was to reduce the action transmitted from the ground to the superstructure represented by mass m_2 and the elastic second element.

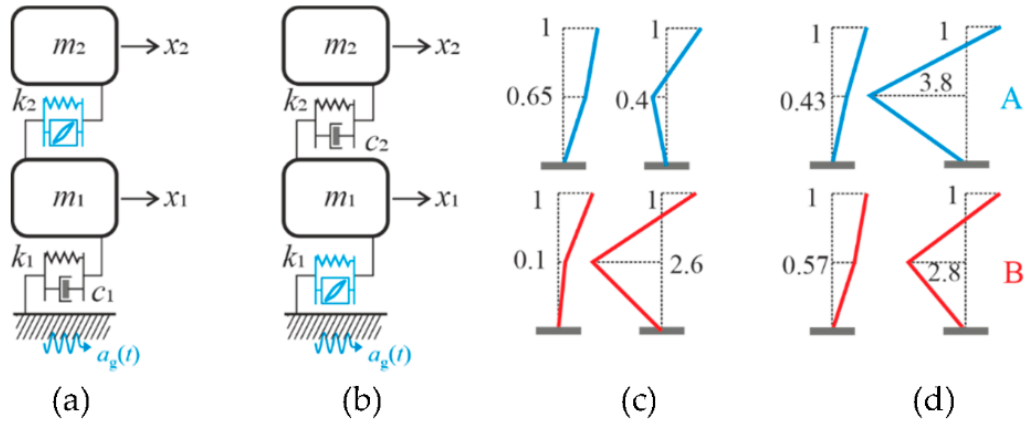

Figure 3. 2DOF system schemes: (**a**) top-hysteresis (TC); (**b**) base-hysteresis configurations (BC), examples of modes at small (A) and large (B) amplitudes; (**c**) TC2; (**d**) BC1.

The equations of motion which govern the forced vibrations of the two systems are two dynamic equilibrium equations of the two masses and the differential equation which describes the hysteretic restoring force, leading to a five first-order differential equations in the state space.

In the case of the TC scheme, Figure 3a, the equations of motion are:

$$m_1\frac{d^2x_1}{dt^2} + k_1x_1 - k_2(x_2 - x_1) + c_1\frac{dx_1}{dt} - z(x_2 - x_1) = -m_1a_g\sin(\Omega t) \tag{8}$$

$$m_2\frac{d^2x_2}{dt^2} + k_2(x_2 - x_1) + z(x_2 - x_1) = -m_2a_g\sin(\Omega t) \tag{9}$$

$$\frac{dz}{dt} = \left\{k_d - \left[\gamma + \beta\mathrm{sgn}\left(z\frac{d(x_2 - x_1)}{dt}\right)\right]|z|^n\right\}\frac{d(x_2 - x_1)}{dt} \tag{10}$$

where the hysteretic component is a function of the relative displacement between the two masses $(x_2 - x_1)$ and acts on both masses.

In the case of the BC scheme, Figure 3b, the equations of motion are:

$$m_1\frac{d^2x_1}{dt^2} + k_1x_1 - k_2(x_2 - x_1) + z(x_1) = -m_1a_g\sin(\Omega t) \tag{11}$$

$$m_2\frac{d^2x_2}{dt^2} + k_2(x_2 - x_1) = -m_2a_g\sin(\Omega t) \tag{12}$$

$$\frac{dz}{dt} = \left\{k_d - \left[\gamma + \beta\mathrm{sgn}\left(z\frac{dx_1}{dt}\right)\right]|z|^n\right\}\frac{dx_1}{dt} \tag{13}$$

where the hysteretic component acts on the mass m_1 only. The initial and post-elastic stiffnesses of the hysteretic element of the 2DOF oscillators are:

$$k_A = k_i + k_d,\ k_B = k_i \tag{14}$$

where $i = 1, 2$ for the base and top configurations, respectively.

Modal Features

The hysteretic device introduced strong nonlinearity in the dynamic response of this type of oscillator. This means that the modal characteristics of the system in both the TC and BC configurations essentially depended on the response amplitude. As shown in [7], when the oscillation amplitudes were small, the hysteretic element exhibited an approximately linear behavior with stiffness k_A, Equation $(14)_1$. Conversely, when the amplitudes of oscillation were large, the hysteretic element exhibited an approximately linear behavior with stiffness k_B, Equation $(14)_2$. Two limit linear systems can therefore be identified: System A and System B, obtained by replacing the hysteretic element with a linear spring with stiffness k_A and k_B, respectively. As the response amplitude varies, the resonance frequency can be approximated by considering, in the place of the hysteretic element, a spring of which the stiffness k_e depends on the amplitude, according to Equation (6), $k_A \geq k_e \geq k_B$. Since the ratio between the two frequencies also depends on the response amplitude, depending on the mechanical parameters of the system, internal resonance conditions $n : m$ ($n\omega_1 \cong m\omega_2$, n and m integers) can easily arise. In such conditions, the response to the harmonic force is strongly modified by the nonlinear modal coupling.

In the following, due to the change in a period of the nonlinear modal shapes, the concept of *nonlinear modal shape* (NMS) is introduced; it represents the configuration of the system at one specific instant, as defined in [7]. This is also useful in characterizing the resonance response of the hysteretic oscillator at each excitation intensity. It is worth noticing that the NMSs can be compared with the linear modes by observing that for increasing amplitude they pass from the modal shapes of system A to those of system B.

Systems in the two configurations, TC and BC, will be examined below; the related mechanical and constitutive parameters are shown in Table A2 of the Appendix A. By way of example, Figure 3c,d report the modes of system A and system B in the case of an oscillator, respectively, with top and base configurations.

4. The Phenomenon of Modal Coupling

Nonlinearity creates the possibility for interaction among modes that are no longer orthogonal. In particular, in the presence of strong nonlinearities, peculiar dynamic phenomena occur through bifurcations of the steady-state motions. This subject is developed in the following, dealing separately with the cases of top and base configurations.

4.1. Top-Hysteresis Configuration (TC)

The top-hysteresis configuration models a primary structure, represented by the mass m_1, connected to the base, and an attachment, represented by the mass m_2, connected to the main structure with a hysteretic element. The hysteretic device, when properly designed, can mitigate the vibrations of the main structure using a mass m_2 which is much smaller than m_1 (light attachment). In the linear field, the importance of the Den Hartog viscoelastic tuned mass damper (TMD) [34,35] is well recognized. By adding a linear attachment with proper parameters, the peak exhibited by the FRC of the primary system response could be divided into two much lower peaks of equal value.

In recent years, much work has been devoted to nonlinear attachments after the pioneering work of [36]; however, few of these have dealt with hysteretic devices [3,4,6,37–42] or related to friction damping [43]. In the following, a hysteretic vibration absorber (HVA) was adopted, and therefore, the calibration of the parameters should be more accurate. In fact, as seen in the previous section, the 2DOF resonance frequencies depend on the oscillation amplitude; thus, at the design stage, it is necessary to take into account the oscillation amplitudes reached by the primary system to obtain the suitable frequency ratio ω_2/ω_1 that is close to optimal.

In order to simulate the behavior of the TMD, it is necessary to tune the characteristics of the added mass m_2 and of the constitutive law so that the frequency of the primary system is similar to that of the hysteretic attachment, approaching the 1:1 internal resonance condition. This requires greater attention, as shown by the analysis of the following cases.

Figure 4 depicts the response to the harmonically excited 2DOF system TC1; its mechanical characteristics are provided in Table A2 of the Appendix A. The system presents a ratio of the initial frequencies $\omega_{2A}/\omega_{1A} \cong 1.3$, which is greater than the optimal value of 1.25 of the TMD. As the amplitude increases, the frequency ratio approaches optimum, leading to a reduction in the response for a definite range of forcing amplitudes.

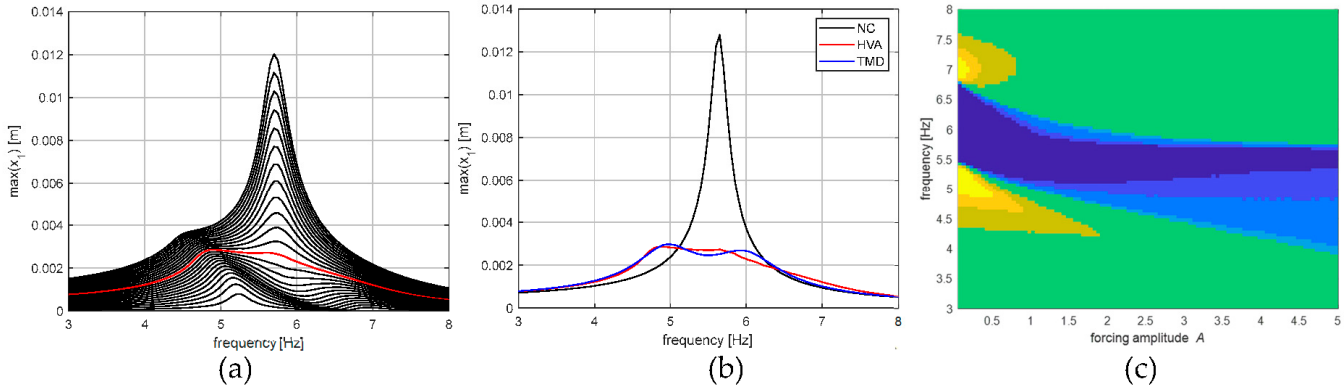

Figure 4. TC1 oscillator close to a (1:1) internal resonance $\omega_{2A}/\omega_{1A} \cong 1.3$): (**a**) FRCs of oscillation amplitudes of mass m_1 for increasing intensity (a_g = [0.005–0.125]g); (**b**) non controlled (black), HVA (red) and TMD (blue) responses at a_g = 0.065g; (**c**) color map comparing the maximum displacements of NC and HVA oscillators (cold colors reveal amplitude reductions and warm colors reveal amplitude increments).

The frequency response curves of the primary structure displacement are reported in Figure 4a with increasing excitation. For the optimal operation of the HVA, in analogy with the behavior of the TMD, the external excitation should generate two equal peaks in the FRC of m_1; this occurs for $a_g = 0.065g$, which corresponds with the red curve in Figure 4a,b. For lower intensities, the equivalent stiffness k_e of the device is lower than the optimal stiffness value of TDM, and as a result, the first peak exceeds the second. On the other hand, for larger amplitudes, the equivalent stiffness of the device exceeds the optimal stiffness of the TMD, and consequently, the second peak predominates. When the amplitude of the external excitation is close to $a_g = 0.065g$, the ratio $\frac{\omega_2}{\omega_1}$ of the system with a hysteretic attachment is close to the value of the optimal visco-elastic tuned mass damper. At this level of excitation, the HVA is as effective as the TMD; in fact, in Figure 4b, there is an 80% reduction in the oscillation amplitudes compared to those that would occur on the non-controlled primary structure (NC). As shown in Figure 4c, the effectiveness of the HVA is maintained even for higher values of the external intensity, provided that the driven frequency is close to the first resonance. In Figure 4c, by means of a color map, the maximum displacements of the NC and HVA oscillators are compared for different forcing intensities and frequencies: blue dots refer to reductions of 40 to 85% with respect to the non-controlled case; green dots are related to slight variations and warm colors indicate the cases where the HVA is not beneficial and leads to an increase in the response, even though this is in a small range of low excitation intensities (yellow regions).

In the previous case of internal resonance 1:1, a hysteretic nonlinear attachment used to reduce the vibrations of the primary structure, simply simulates the behavior of the classic TMD; therefore, the results described above are similar to what has already been observed within the framework of linear dynamics. Although the advantage of this device lies in its simplicity because hysteretic elements combine elastic and dissipative capacities without the need for a viscous damper [41], the effectiveness is, however, limited to definite excitation intensities. Furthermore, the nonlinearity resides in the constitutive law of the attachment. However, no typical phenomena of nonlinear dynamics are triggered; this novel contribution could be usefully investigated for the mitigation of vibrations, as illustrated below.

The occurrence of internal resonance conditions n:1, with $n > 1$ integer [43–46], is more interesting, and the relevant phenomena can be exploited to achieve a reduction in the forced response for certain values of excitation and frequency, as shown in the following. As the hysteretic restoring force is a highly nonlinear constitutive law, various internal resonance conditions are likely to occur. In the following, an oscillator that undergoes a 2:1 internal resonance was analyzed, Figure 5. Similar outcomes could be observed for $n > 2$ and also for other internal resonance conditions of the kind $n\omega_1 \cong m\omega_2$.

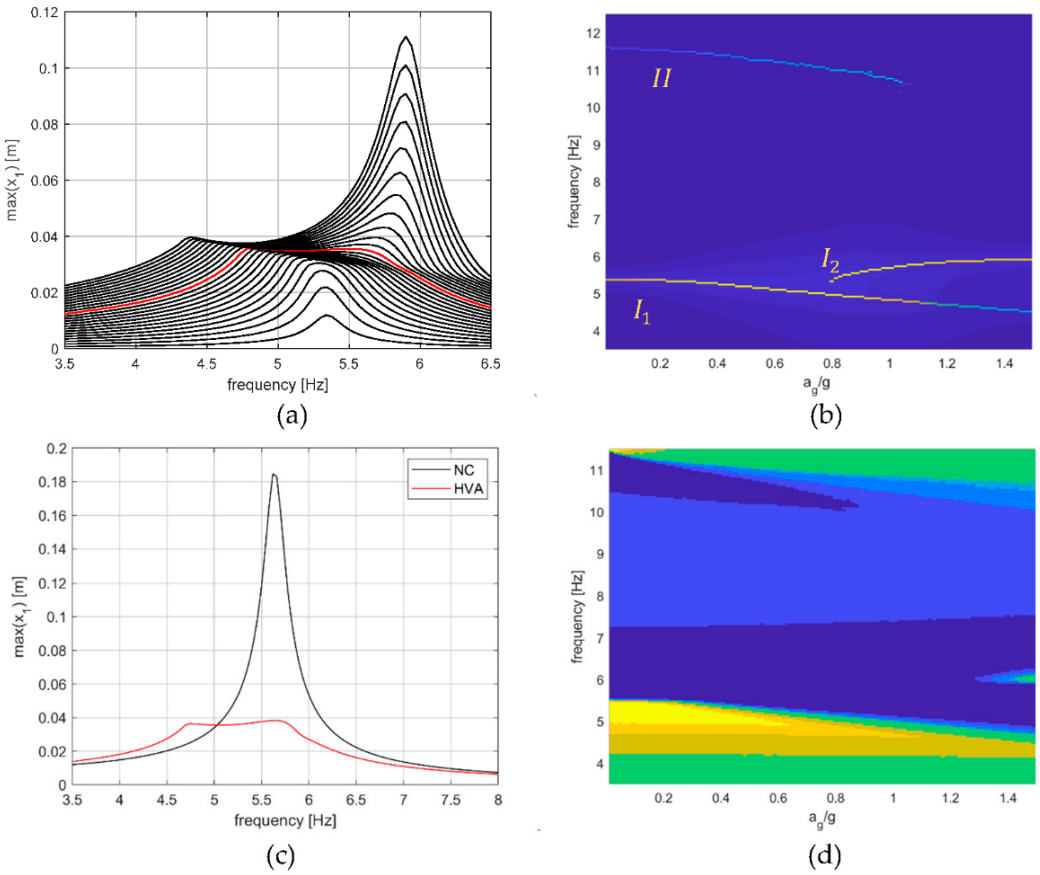

Figure 5. TC2 oscillator close to a (2:1) internal resonance ($\omega_{2A}/\omega_{1A} \cong 2.15$, $\omega_{2B}/\omega_{1B} \cong 1.46$): (**a**) FRCs of oscillation amplitudes of mass m_1 for increasing intensity (a_g = [0.025–1.5]g), optimal excitation $a_g = 0.83g$ (red curve); (**b**) color map of the maximum response normalized to the excitation amplitude for different excitation frequencies and intensities (warm colors reveal peaks related to modes); (**c**) non-controlled (NC) and HVA responses at $a_g = 0.83g$; (**d**) Color map comparing the maximum displacements of NC and HVA oscillators (cold colors reveal amplitude reductions, warm colors relate to amplitude increments, and green is related to slight variations).

On the same main structure of the TC1 system, an HVA was applied with mass m_2, and the stiffness k_2 was calibrated in order to obtain a frequency ratio close to 2:1; the mechanical parameters of this oscillator (TC2) are reported in Table A2 of the Appendix A. In Figure 5a, the FRCs of the primary mass displacement is reported with increasing excitation intensity. For low intensities, the resonance frequencies were close to those of linear system A (ω_{1A} = 5.35 Hz, ω_{2A} = 11.5 Hz, with an initial value $r_A = \omega_{2A}/\omega_{1A} \cong 2.15$); for high intensities, the resonance frequencies were close to those of linear system B (with a final ratio $r_B = \omega_{2B}/\omega_{1B} \cong 1.5$). For intermediate intensities, the ratio approached the internal resonance condition 2:1, where the FRC around the first mode experienced a bifurcation and, instantaneously, the curve of the 2DOFs system showed two peaks (I_1 and I_2), in addition to the peak related to the second resonance (II), which was much

smaller due to the distribution of excitation, the projection of which was limited on the second mode.

In more detail, the I_1 peak, corresponding to the first resonance frequency, doubled, following a trend that recalls the response of the VMTD and the previous TC1 system. However, unlike those cases, a typical bifurcation scenario of the nonlinear dynamic response was activated here. In fact, in the TC2 system, the rise of the I_2 peak in the FRC is related to a novel superabundant mode generated by a bifurcation associated with an internal 2:1 resonance. An insight into this phenomenon is provided by the color map in Figure 5b, where, for different excitation amplitudes and frequencies, the resonance amplitudes of the m_1 steady-state responses are evidenced. For small excitation amplitudes, two branches develop, starting from the two linear frequencies A. At the critical value of $a_g = 0.79g$, the novel mode related to I_2 arises. For increasing excitation intensity, the value of peak I_2 equals that of peak I_1 at $a_g = 0.83g$ (red curve) and then prevails. Along the branch I_1 the nonlinear modal shape evolves passing from the linear mode A, for small excitation, to the linear mode B, for high excitation, Figure 3c. Similarly, the nonlinear modal shape of the superabundant mode evolves reaching the linear mode B, Figure 3c. At $a_g = 0.83g$, when the two peaks I_1 and I_2 are equivalent, the reduction in the vibration amplitude of the main structure reaches its maximum, about 80% with respect to the non-controlled case, Figure 5c. Then, the optimal excitation can be assumed as that which produces an extra peak I_2, equal to the preexistent one I_1 in the FRC of m_1. For different forcing intensities, the hysteretic absorber mitigated the system vibrations as well: as shown in Figure 5d, the effectiveness of the HVA was maintained in a wide range of intensities and frequencies (blue regions).

4.2. Base-Hysteresis Configuration (BC)

To explore the ability of a hysteretic isolator to reduce the transmission of excitation from the base to the superstructure by nonlinear modal coupling, the system with a hysteretic element at the base (Figure 3b) and with the BC1 characteristics (reported in Table A2 of the Appendix A), is considered in Figure 6. The small amplitude frequencies were ω_{1A} = 3.89 Hz and ω_{2A} = 11.32 Hz with a ratio ω_{2A}/ω_{1A} = 2.90, which are close to the internal resonance condition 3:1.

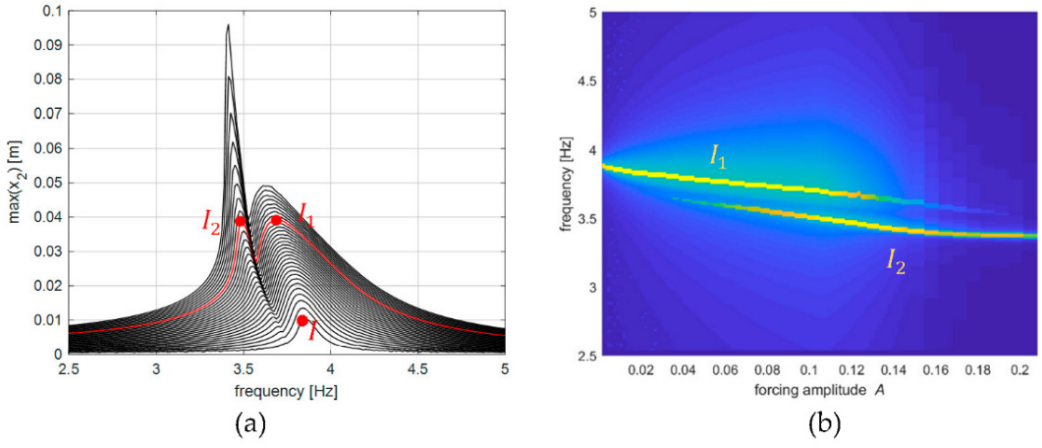

Figure 6. BC1 oscillator close to a (3:1) internal resonance ($\omega_{2A}/\omega_{1A} \cong 2.90$, $\omega_{2B}/\omega_{1B} \cong 3.0$): (**a**) FRCs around the first resonance for increasing excitation amplitude (A = 0.007–0.14), optimal intensity A = 0.10 (red); (**b**) color map of the maximum response normalized to the excitation amplitude for different excitation frequencies and intensities (warm colors reveal peaks related to modes).

Figure 6a focuses on the FRCs of the m_2 displacement amplitude centered on the first resonance. Initially, for small excitation intensities, the single peak I is present close to the first natural frequency; however, with increasing intensity, at the critical value $A = 0.024$,

a second peak I_2 appears which grows until it reaches I_1, at $A = 0.1$ (red *FRC curve*), and then overcomes it. As shown by the color map in Figure 6b, the fundamental branch ω–A of the first resonance experiences a bifurcation and then shows a new branch in addition to the preexisting one, which is destined to disappear; the new branch I_2 is the only surviving one for large excitation intensities.

It is worth noticing that the nonlinear modal trajectories in the physical plane $x_1 - x_2$, related to the steady-state responses of I_1 and I_2, always exhibit opposite curvatures. This is shown in Figure 7: the novel mode I_2 arises at $A = 0.024$, showing a $\int$-shaped modal trajectory, whereas the preexisting mode I_1 exhibits a $\wr$-shaped one; as soon as I_2 prevails over I_1 ($A > 0.1$), its modal trajectory becomes $\wr$-shaped, while the other turns $\int$-shaped and disappears. Finally, along both branches, the nonlinear modal shapes evolve, passing from the linear mode A, for small excitation, to the linear mode B, for high excitation, Figure 3d.

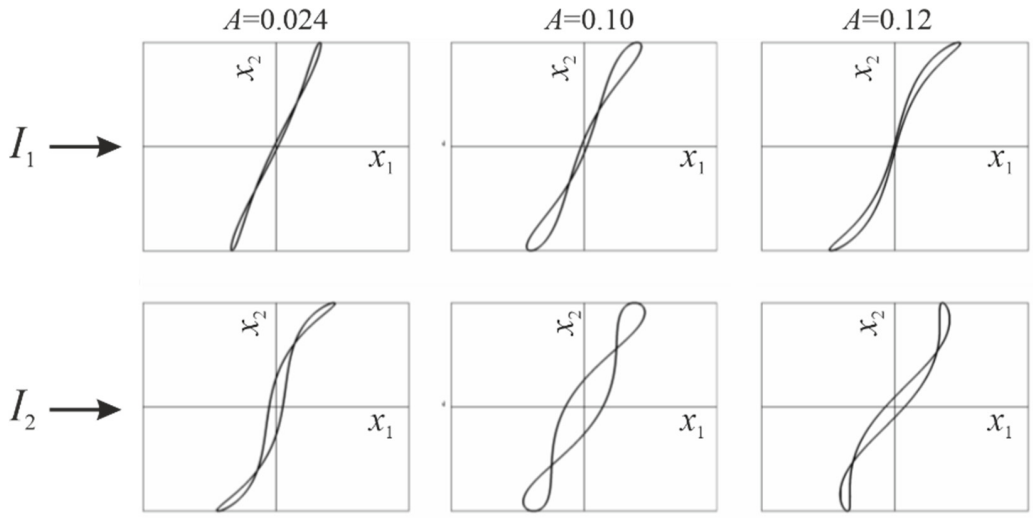

Figure 7. BC1 oscillator: evolution of the modal trajectories in the physical plane related to peaks I_1 and I_2 as excitation increases.

The comparison of the dynamic behavior of two different systems, BC1, close to an internal resonance condition 3:1, and BC1n, far from an internal resonance condition (Table A2 in the Appendix A) with a frequency ratio $\omega_{2A}/\omega_{1A} = 3.40$, makes it possible to clearly illustrate the favorable effects of nonlinear modal interactions [1,2,29]. For BC1n, in this case, there is only a single branch related to the first resonance, Figure 8a, which, as expected, occurs at lower frequencies for increasing forcing intensities due to hysteretic softening. On the contrary, the maximum displacement of the two masses is much smaller for the system BC1 in conditions of internal resonance, with a reduction of about 70% for m_2 with respect to the non-resonant case (BC1n), Figure 8b. As shown in Figure 8c, the closeness to internal resonance conditions leads to a relevant displacement reduction in a wide range of forcing frequency and amplitude in the blue regions.

Internal resonance conditions n:1 with n even can also occur. As an example, a BC2 system close to internal resonance 2:1 is considered in Figure 9.

At small intensities, the amplification of the second mode II is much smaller than the first I_1 due to the distribution of excitation. For increasing intensity, Figure 9a, the zone of the first resonance widens, and a novel peak I_2 emerges and reaches the peak I_1 near $A = 0.32$, leading to a flattening of the FRCs, with a notable reduction in the first resonance peaks in a large range of force intensities. The resonance amplitudes of the m_2 steady-state responses are evidenced in Figure 9b for different excitation amplitudes and frequencies: the branches related to the peaks I_1, I_2 and II are well-evidenced, together with a short branch of superharmonic solutions arising for low excitation frequencies.

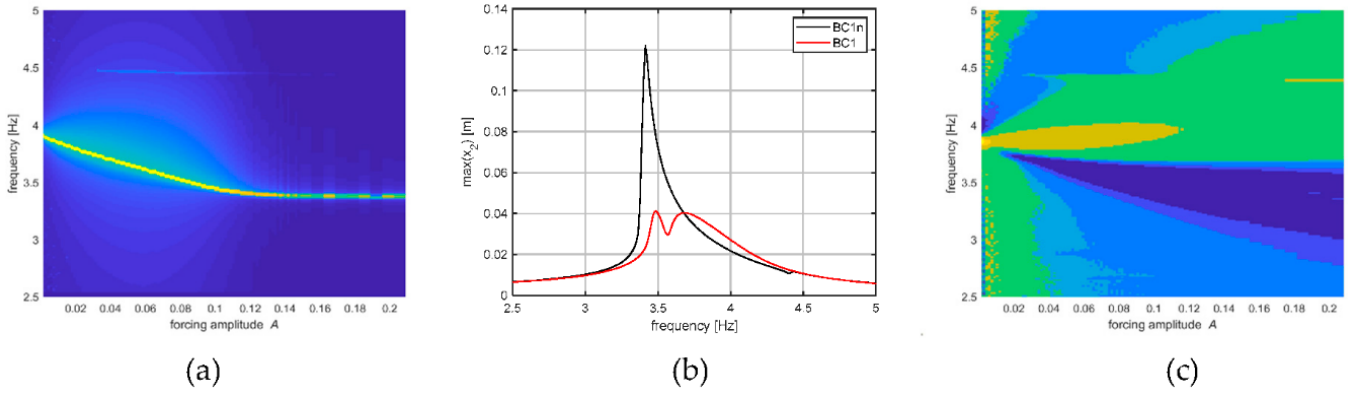

Figure 8. (**a**) color map of the maximum response of non-resonant system BC1n for different forcing frequencies and intensities; (**b**) non-resonant (BC1n) and resonant (BC1) FRCs responses at $A = 0.10$; (**c**) color map comparing the maximum displacements of BC1 and BC1n oscillators (cold colors reveal amplitude reductions, warm colors indicate amplitude increments, green indicates slight variations).

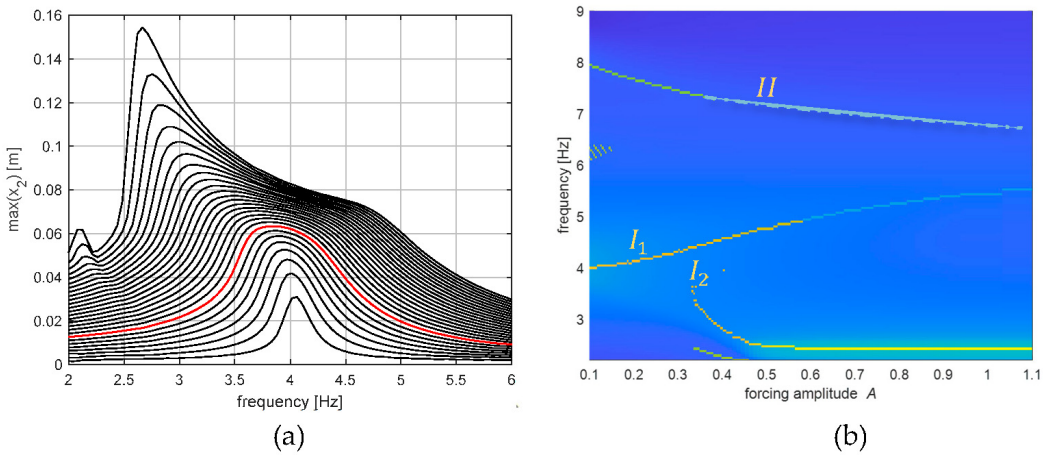

Figure 9. BC2 oscillator close to (2:1) internal resonance ($\omega_{2A}/\omega_{1A} \cong 2.09$): (a) FRCs for increasing force intensity ($A = 0.015$–0.4), red $A = 0.32$; (**b**) color map highlighting the main branches.

5. Conclusions

The aim of this paper is to investigate nonlinear modal interactions in multidegree-of-freedom systems with hysteresis in view of exploiting this phenomenon to achieve mitigation of the forced response. In particular, a simple 2DOF structure that consisted of two masses and two elements, one elastic and one hysteretic, was investigated by considering two different configurations: top configuration, with the hysteretic element at the top (TC) between the two masses; and base configuration (BC), with the hysteretic element at the base.

The nonlinearity of the hysteretic element is described by the Bouc–Wen model and can be classified as a strong nonlinearity due to the notable dependence of stiffness and damping on the oscillation amplitude. The main dynamic effects of hysteresis are first illustrated by the FRCs of a SDOF hysteretic system under harmonic excitation. The FRCs were always single-valued functions, which meant that the steady-state solutions were always stable for the full hysteresis model considered. Due to the reduction in stiffness with amplitude, the nonlinearity was of the softening type: the resonance frequency decreased from ω_A for small amplitudes, to ω_B for high amplitudes, where ω_A and ω_B were the frequencies of the linear oscillator with a stiffness that was, respectively, equal to the initial and post-elastic stiffness of the hysteretic element.

The nonlinear behavior the 2DOF system, as already observed for the SDOF, is again comprised between those of two linear systems: system A for small amplitudes, system B for large amplitudes. The modal properties of the system change with the oscillation amplitude. Accordingly, natural frequencies, and their ratio, changed and the conditions

of internal resonance, where the phenomena of nonlinear interaction are exalted, were easily met.

For the top configuration, first, the case where the hysteretic device had a frequency close to that of the main structure was considered, which recalled the case of the well-known tuned mass damper. The hysteretic element, which combined stiffness and dissipation characteristics, made it possible to avoid the viscous device, but the performance was similar to that of the viscoelastic damper, only in a certain range of force intensity, due to the dependence on the oscillation amplitude.

However, the introduction of a hysteretic element could take advantage of the phenomena of nonlinear interactions, which occurred when the system was close to internal resonance conditions n:1 with $n > 1$. The 2:1 condition was investigated for TC systems, and the 3:1 and 2:1 conditions were investigated for BC systems. A large variety of behaviors were observed; however, concerning the beneficial effects in vibration mitigation, similar outcomes were found for both configurations. At a certain force intensity, the FRCs around the resonance of the first mode exhibited a bifurcation with the arising of a novel mode. The existence of two resonant peaks around the first mode was the result of the involvement of the second mode, which strongly modified the modal trajectories and, mainly, the response amplitude.

In conclusion, the novel contribution of the paper is the enlightenment of the use of hysteretic devices, which offers the possibility of increasing the dissipation characteristics of the system and, at the same time, due to its intrinsic nonlinear behavior, facilitates the transfer of energy from the mode, directly excited to the other not directly excited, with appreciable mitigation of vibrations of the structure.

Author Contributions: Conceptualization, P.C. and F.V.; methodology, P.C. and F.V.; software, P.C.; supervision, F.V. All authors have read and agreed to the published version of the manuscript.

Funding: This work has been partially supported by the MIUR (Ministry of Education, University and Research) under the grant PRIN 2017-N. 2017L7X3CS.

Institutional Review Board Statement: Not applicable.

Informed Consent Statement: Not applicable.

Data Availability Statement: Not applicable.

Conflicts of Interest: The authors declare no conflict of interest. The funders had no role in the design of the study; the collection, analyses, or interpretation of data; the writing of the manuscript; or in the decision to publish the results.

Appendix A

In the following tables, the parameters of the SDOF and 2DOF hysteretic systems investigated in this paper are reported.

Table A1. Mechanical characteristics of SDOF systems.

SDOF Name	m_1 kg	k_1 kN/m	δ	γ [1/m]	γ/β	k_A kN/m	f_y kN	x_y m
BW1	600	440	0.3	55	1	1466.7	13.3	0.0091
BW2	600	440	0.3	100	10	1466.7	13.3	0.0091

Table A2. Mechanical characteristics of 2DOF systems.

2DOF Name	m_1 kg	m_2 kg	k_1 kN/m	k_d kN/m	γ [1/m]	γ/β	δ	ζ_1	k_2 kN/m	ζ_2	ω_{1A} Hz	ω_{2A} Hz
TC1 1:1	1220	61	1532.6	82	82	1	0.14	0.02	14.51	0	5.27	6.95
TC2 2:1	1220	101	1532.6	408	55	1	0.15	0.02	72	0	5.35	11.5

Table A2. *Cont.*

2DOF Name	m_1 kg	m_2 kg	k_1 kN/m	k_d kN/m	γ [1/m]	γ/β	δ	ζ_1	k_2 kN/m	ζ_2	ω_{1A} Hz	ω_{2A} Hz
BC1 3:1	256	420	440	300	55	1	0.6	0	440	0.01	3.89	11.32
BC1n	256	420	353	1606	55	1	0.6	0	889	0.01	3.93	13.3
BC2 2:1	1220	549	440	2493	55	1	0.15	0	440	0.01	4.1	8.57

References

1. Jing, X.J.; Vakakis, A. Exploring nonlinear benefits in engineering. *Mech. Syst. Signal Process.* **2019**, *125*, 1–3. [CrossRef]
2. Vakakis, A.F. Intentional utilization of strong nonlinearity in structural dynamics. *Proc. Eng.* **2017**, *199*, 70–77. [CrossRef]
3. Ture Savadkoohi, A.; Lamarque, C.-H.; Contessa, M.V. Trapping vibratory energy of main linear structures by coupling light systems with geometrical and material non-linearities. *Int. J. Non-Linear Mech.* **2016**, *80*, 3–13. [CrossRef]
4. Vestroni, F.; Casini, P. Mitigation of structural vibrations by hysteretic oscillators in internal resonance. *Nonlinear Dyn.* **2020**, *99*, 505–518. [CrossRef]
5. Liang, Z.; Lee, G.C.; Dargush, G.F.; Song, J. *Structural Damping: Applications in Seismic Response Modification*; CRC Press: Boca Raton, FL, USA, 2011.
6. Casalotti, A.; Lacarbonara, W. Tailoring of pinched hysteresis for nonlinear vibration absorption via asymptotic analysis. *Int. J. Non-Linear Mech.* **2017**, *94*, 59–71. [CrossRef]
7. Casini, P.; Vestroni, F. Nonlinear resonances of hysteretic oscillators. *Acta Mech.* **2018**, *229*, 939–952. [CrossRef]
8. Tsiatas, G.C.; Charalampakis, A.E. A new hysteretic nonlinear energy sink (HNES). *Commun. Nonlinear Sci. Numer. Simul.* **2018**, *60*, 1–11. [CrossRef]
9. Basili, M.; Casini, P.; Morelli, L.; Vestroni, F. Vibration Mitigation of Rail Noise Barriers by Hysteretic Absorbers. *J. App. Comp. Mech.* **2021**, *7*, 1205–1217.
10. Nayfeh, A.H.; Balachandran, B. *Applied Nonlinear Dynamics: Analytical, Computational, and Experimental Methods*; Wiley: New York, NY, USA, 1995.
11. Vakakis, A.F. Non-linear normal modes and their applications in vibration theory: An overview. *Mech. Syst. Signal Process.* **1997**, *11*, 3–22. [CrossRef]
12. Vestroni, F.; Luongo, A.; Paolone, A. A perturbation method for evaluating nonlinear normal modes of a piecewise linear 2-DOF system. *Nonlinear Dyn.* **2008**, *54*, 379–393. [CrossRef]
13. Wiercigroch, M.; de Kraker, B. *Applied Nonlinear Dynamics and Chaos of Mechanical Systems with Discontinuities*; World Scientific Series in Nonlinear Science, Series A; World Scientific: Singapore, 2000; Volume 28.
14. Awrejcewicz, J.; Dzyubak, L.; Lamarque, C.H. Modelling of hysteresis using Masing–Bouc-Wen's framework and search of conditions for the chaotic responses. *Commun. Nonliner Sci. Numer. Simul.* **2008**, *13*, 939–958. [CrossRef]
15. Rand, R.H.; Pak, C.H.; Vakakis, A.F. Bifurcation of nonlinear normal modes in a class of two degree of freedom systems. *Acta Mech.* **1992**, *3*, 129–145.
16. Casini, P.; Vestroni, F. Characterization of bifurcating Nonlinear Normal Modes in piecewise linear mechanical systems. *Int. J. Non-Linear Mech.* **2011**, *46*, 142–150. [CrossRef]
17. Vestroni, F.; Noori, M. Hysteresis in mechanical systems: Modeling and dynamic response. *Int. J. Non-Linear Mech.* **2002**, *37*, 1261–1262. [CrossRef]
18. Al-Bender, F.; Symens, W.; Swevers, J.; Van Brussel, H. Theoretical analysis of the dynamic behavior of hysteresis elements in mechanical systems. *Int. J. Non-Linear Mech.* **2004**, *39*, 1721–1735. [CrossRef]
19. Masuda, A.; Noori, M. Optimization of hysteretic characteristics of damping devices based on pseudoelastic shape memory alloys. *Int. J. Non-Linear Mech.* **2002**, *37*, 1375–1386. [CrossRef]
20. Lacarbonara, W.; Vestroni, F. Nonclassical responses of oscillators with hysteresis. *Nonlinear Dyn.* **2003**, *32*, 235–258. [CrossRef]
21. Xiong, H.; Kong, X.; Li, H.; Yang, Z. Vibration analysis of nonlinear systems with the bilinear hysteretic oscillator by using incremental harmonic balance method. *Commun. Nonlinear Sci. Numer. Simul.* **2017**, *42*, 437. [CrossRef]
22. Vaiana, N.; Sessa, S.; Marmo, F.; Rosati, L. Nonlinear dynamic analysis of hysteretic mechanical systems by combining a novel rate-independent model and an explicit time integration method. *Nonlinear Dyn.* **2019**, *98*, 2879–2901. [CrossRef]
23. Pak, C.H. On the stability behaviour of bifurcated normal modes in coupled nonlinear systems. *J. Appl. Mech.* **1989**, *56*, 155–161. [CrossRef]
24. Masiani, R.; Capecchi, D.; Vestroni, F. Resonant and coupled response of hysteretic two-degree-of-freedom systems using harmonic balance method. *Int. J. Non-Linear Mech.* **2002**, *37*, 1421–1434. [CrossRef]
25. Visintin, A. *Differential Models of Hysteresis*; Springer: Berlin/Heidelberg, Germany, 1994.
26. Antonelli, M.; Carboni, B.; Lacarbonara, W.; Bernardini, D.; Kalmar-Nagy, T. Quantifying Rate-Dependence of a Nonlinear Hysteretic Device. In *Nonlinear Dynamics of Structures, Systems and Devices, Proceedings of the 1st International Nonlinear Dynamics Conference, NODYCON, Rome, Italy, 17–19 February 2019*; Springer: Cham, Switzerland, 2020; pp. 347–355.

27. Bouc, R. Forced vibrations of mechanical systems with hysteresis. In Proceedings of the Fourth Conference on Nonlinear Oscillations, Prague, Czech Republic, 5–9 September 1967.
28. Wen, Y.K. Method of random vibration of hysteretic systems. *ASCE J. Eng. Mech.* **1976**, *102*, 249–263. [CrossRef]
29. Ni, Y.Q.; Ko, J.M.; Wong, C.W. Identification of non-linear hysteretic isolators from periodic vibration tests. *J. Sound Vibr.* **1998**, *217*, 747–756. [CrossRef]
30. Ismail, M.; Ikhouane, F.; Rodellar, J. The Hysteresis Bouc-Wen Model, a Survey. *Arch. Comput. Methods Eng.* **2009**, *16*, 161–188. [CrossRef]
31. Zhang, Z.; Tian, X.; Ge, X. Dynamic Characteristics of the Bouc–Wen Nonlinear Isolation System. *Appl. Sci.* **2021**, *11*, 6106. [CrossRef]
32. Vestroni, F.; Casini, P. Nonlinear dynamics and phenomena in oscillators with hysteresis. In *Modern Trends in Structural and Solid Mechanics*; Challamel, N., Kaplunov, J., Takewaki, I., Eds.; ISTE: London, UK; Wiley: Hoboken, NJ, USA, 2021.
33. Capecchi, D.; Vestroni, F. Periodic response of a class of hysteretic oscillators. *Int. J. Non-Linear Mech.* **1990**, *25*, 309–317. [CrossRef]
34. Den Hartog, J.P. *Mechanical Vibrations*; McGraw-Hill: New York, NY, USA, 1934.
35. Dai, J.; Xu, Z.D.; Gai, P.P. Dynamic analysis of viscoelastic tuned mass damper system under harmonic excitation. *J. Vib. Control* **2019**, *25*, 1768–1779. [CrossRef]
36. Vakakis, A.F.; Manevitch, L.; Gendelman, O.; Bergman, L. Dynamics of linear discrete systems connected to local, essentially non-linear attachments. *J. Sound Vib.* **2003**, *264*, 559–577. [CrossRef]
37. Laxalde, D.; Thouverez, F.; Sinou, J.J. Dynamics of a linear oscillator connected to a small strongly non-linear hysteretic absorber. *Int. J. Non-Linear Mech.* **2006**, *41*, 969–978. [CrossRef]
38. Zeynalian, M.; Ronagh, H.R.; Dux, P. Analytical Description of Pinching, Degrading, and Sliding in a Bilinear Hys-teretic System. *J. Eng. Mech.* **2012**, *138*, 1381–1387.
39. Carpineto, N.; Lacarbonara, W.; Vestroni, F. Hysteretic tuned mass dampers for structural vibration mitigation. *J. Sound Vib.* **2013**, *333*, 1302–1318. [CrossRef]
40. Carboni, B.; Lacarbonara, W. Nonlinear dynamic characterization of a new hysteretic device: Experiments and computations. *Nonlinear Dyn.* **2016**, *83*, 23–39. [CrossRef]
41. Bagheri, S.; Rahmani-Dabbagh, V. Seismic response control with inelastic tuned mass dampers. *Eng. Struct.* **2018**, *172*, 712–722. [CrossRef]
42. Salvatori, A.; Carboni, B.; Lacarbonara, W. Nonlinear dynamic response of an isolation system with superelastic hysteresis and negative stiffness. *Nonlinear Dyn.* **2022**, *107*, 1765–1790. [CrossRef]
43. Krack, M.; Bergman, L.A.; Vakakis, A.F. On the efficacy of friction damping in the presence of nonlinear modal interactions. *J. Sound Vib.* **2016**, *370*, 209–220. [CrossRef]
44. Jo, H.; Yabuno, H. Amplitude reduction of primary resonance of nonlinear oscillator by a dynamic vibration absorber using nonlinear coupling. *Nonlinear Dyn.* **2009**, *55*, 67–78. [CrossRef]
45. Ji, J.C. Design of a nonlinear vibration absorber using three-to-one internal resonances. *Mech. Syst. Signal Process.* **2014**, *42*, 236–246. [CrossRef]
46. Casini, P.; Vestroni, F. The role of the hysteretic restoring force on modal interactions in nonlinear dynamics. *Int. J. Non-Linear Mech.* **2022**, *143*, 104029. [CrossRef]